Optical Materials 55 (2016) 102–108

Contents lists available at ScienceDirect

Optical Materials

journal homepage: www.elsevier.com/locate/optmat

Polarization controlled intensity noise correlation and squeezing of four-wave mixing processes in rubidium vapor

Changbiao Li [a,*], Zihai Jiang [a], Xiuxiu Wang [a], Irfan Ahmed [a,b], Faizan Raza [a], Yiheng Yang [a], Yanpeng Zhang [a,*]

[a] Key Laboratory for Physical Electronics and Devices of the Ministry of Education & Shaanxi Key Lab of Information Photonic Technique, Xi'an Jiaotong University, Xi'an 710049, China

[b] Electrical Engineering Department, Sukkur Institute of Business Administration, Airport Road, Sukkur 65200, Pakistan

ARTICLE INFO

Article history:
Received 22 January 2016
Received in revised form 14 March 2016
Accepted 15 March 2016

OCIS:
(190.4380) Nonlinear optics, four-wave mixing
(160.4330) Nonlinear optical materials
(270.6570) Squeezed states

Keywords:
Intensity noise correlation
Squeezing
Four-wave mixing process

ABSTRACT

We observed four-wave mixing (FWM) processes in a double-Λ level of rubidium atomic system with electromagnetically induced transparency window having different polarization. The Autler-Townes splitting of FWM induced by the polarized multi-dark-state is observed. And the two-stage line shape of correlation that exhibits a sharp peak and a broad peak is also studied. The sharp peak and the broad peak are from the correlation of two spontaneous parametric FWMs and that of the vertical component and horizontal component of two coherent FWMs. Moreover we demonstrate that the intensity noise correlation and intensity-difference squeezing can be well modulated by the relative initial phase and nonlinear phase shift. Meanwhile, we also found the following of correlation (anti-correlation) by intensity-difference squeezing (anti-squeezing). The associated results may be applicable in all-optical communication and optical information processing on photonic chips.

1. Introduction

Recently, electromagnetically induced transparency (EIT) is used to investigate nonlinearities with exploitation coherent effect [1,2]. And EIT in an atomic medium has attracted a great deal of attention in the last two decades because of the wide range of potential applications in lasing without inversion, slow light, photon manipulation [3] and information storage, and quantum communications [4]. As, nonlinearities can be significantly enhanced and modified due to atomic coherence in an EIT system [5,6], particularly enhancement multi-wave mixing (MWM) [7]. Currently, EIT, FWM and six-wave mixing (SWM) processes in atomic ensemble are being developed. In the recent few years, probe transmission and the generated dressed MWM are enhanced or suppressed through the dark state and have been demonstrated both in theory and experiment. By changing the polarization properties [8] of the incident light beam, we may bring change in MWM process and define their trade off. Thus by analysis, we have defined relationship between the output intensity and polarization of the incident beams. The relationship between high-order nonlinear polarization [9] and polarization of incident beams have been investigated. In order to verify the changes in MWM signal peak situation by incident light having different polarizations, we have introduced the degenerate Zeeman sublevels [10] subjected to the dressing effects. Intensity correlations and intensity difference squeezing of optical fields propagating were studied [11]. Three-fields noise correlations with two FWM signals as well as the generation of bright correlated Stokes and anti-Stokes light beams have been investigated [12]. Besides, P.D. Lett's group has obtained up to −5.4 dB of intensity-difference squeezing in a hot rubidium atomic system [13]; and W.P. Zhang's group has observed that the maximal degree of intensity-difference squeezing of twin beams from a hot atomic vapor cell can reach around −5.4 ± 0.4 dB [14]. We have not only shown that the intensity-difference squeezing and intensity noise correlation can be easily manipulated by several parameters, but also verified that the correlation and squeezing can be controlled by the nonlinear phase shift caused by the dressing beam.

* Corresponding authors.
E-mail addresses: cbli@mail.xjtu.edu.cn (C. Li), ypzhang@mail.xjtu.edu.cn (Y. Zhang).

http://dx.doi.org/10.1016/j.optmat.2016.03.028
0925-3467/

In this paper, we studied experimentally and theoretically the coexisting multi-level atomic system interactions in FWM process. At the same time, we noticed that $\boldsymbol{E}_1$ and $\boldsymbol{E}_2$ produced spontaneous parametric four-wave mixing (SP-FWM). The induced AT splitting can be controlled by changing polarization and power of the incident beams. We observed the FWM process in the ^{85}Rb atomic vapor that can generate outputs whose noise intensity fluctuations are correlated followed by their intensity difference squeezing. Besides, we also explained the phenomenon of the two-stage line shape of correlation which including the sharp peak correlation (correlation from two SP-FWMs) and the broad peak correlation (correlation from vertical component ($\boldsymbol{E}_{Fs}$), and horizontal component ($\boldsymbol{E}_{Fp}$) of two coherent FWMs). The correlation and squeezing can be controlled by the relative nonlinear phase shift caused by the dressing fields, on the other word, the correlation and squeezing can be switched into anti-correlation and anti-squeezing, respectively. The experimental results are in well agreements with theoretically calculated results.

2. Experimental setup and theoretical model

The experiments are performed in a double-Λ-type three level of ^{85}Rb atomic system as depicted in Fig. 1(a), rubidium atoms can transit from ground to two levels $5S_{1/2}$, from the ground state to the excited state $5S_{1/2}$ and $5P_{2/3}$ lines called D_1 and D_2, respectively. As the hyperfine structure of excited state $5P_{1/2}$ is simple, generally the 795 nm D_1 line is chosen as the transition of mixing process line. Where the three energy levels are labeled as $5S_{1/2}$ ($|1\rangle$, F = 1, $|2\rangle$, F = 2), and $5P_{2/3}$ ($|3\rangle$). Here, the FWM ($\boldsymbol{E}_F$) process occurs in the subsystem ($|3\rangle - |1\rangle$) involving three beams $\boldsymbol{E}_1$, $\boldsymbol{E}_2$ and $\boldsymbol{E}_2'$. $\boldsymbol{E}_F$ propagates in opposite direction of $\boldsymbol{k}_2'$ and satisfies the phase-matching condition $\mathbf{k_F} = \mathbf{k_1} - \mathbf{k_2} + \mathbf{k_2'}$ and the energy conservation $\omega_F = \omega_1 - \omega_2 + \omega_2'$ as shown in Fig. 1(a).

In the experiment, the laser beam $\boldsymbol{E}_1$ (with frequency ω_1, Rabi frequency Ω_1, and wave vector $\boldsymbol{k}_1$) emitted from an external cavity diode laser (ECDL) connects the transition between the energy levels $|1\rangle - |3\rangle$ and serves as the probe beam. The beams $\boldsymbol{E}_2$ and $\boldsymbol{E}_2'$ with the same frequency ω_2 connect the transition between level $|2\rangle$ and $|3\rangle$. Fig. 1(e) shows the geometric structure of the laser beams. $\boldsymbol{E}_2$ and $\boldsymbol{E}_2'$ are in the same direction of $\boldsymbol{E}_1$, where $\boldsymbol{E}_2'$ and $\boldsymbol{E}_2$ both have a small angle (~0.3°) with $\boldsymbol{E}_1$. Fig. 1(d) shows division of FWM into horizontal ($\boldsymbol{E}_{Fp}$) and vertical ($\boldsymbol{E}_{Fs}$) signal through PBS, and their respective intensities are recorded by the avalanche photo detector (APD). Meanwhile, SP-FWM is generated accompanying polarization controlled FWM, and these two detectors also record Stokes ($\boldsymbol{E}_s$) and anti-Stokes ($\boldsymbol{E}_{as}$) signal. Therefore, we can calculate the intensity noise correlation and their degree of intensity difference squeezing using these recorded intensities at APD1 and APD2.

3. Correlation function and intensity-difference squeezing

In nonlinear medium, $\chi^{(3)}$ is a function of the density-matrix elements described by the perturbation chains, so the perturbation chain of FWM is obtained as $\rho_{11}^{(0)} \xrightarrow{E_1} \rho_{31}^{(1)} \xrightarrow{E_2^*} \rho_{21}^{(2)} \xrightarrow{E_2'} \rho_{31}^{(3)}$ and the corresponding density matrix elements for $\boldsymbol{E}_F$ can be written as

$$\rho_{31}^{(3)} = -iG_1G_2^*G_2'/d_{31}^2d_{21}, \tag{1}$$

where $d_{31} = \Gamma_{31} + i\Delta_1$, $d_{21} = \Gamma_{21} + i(\Delta_1 - \Delta_2)$ and $G_i = \mu_i E_i/\hbar$. We define the frequency detuning and Rabi frequencies of different laser beams as $\Delta_i = \Omega_{mn} - \omega_i$ (i = 1, 2, 3) and $G_i = \mu_{mn}E_i/\hbar$ ($G_i' = \mu_{mn}E_i'/\hbar$), where Ω_{mn} and μ_{mn} denote the transition frequency and dipole moment, respectively, between $|m\rangle$ and $|n\rangle$ having transverse relaxation rate Γ_{mn} and E_i is the electrical field intensity. $\kappa \propto \chi_i^{(3)} \propto \rho^{(3)}$, as the relationship predicts, the output

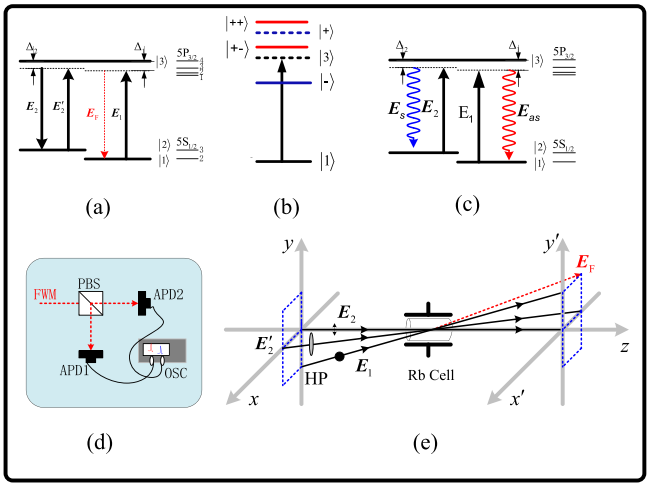

Fig. 1. (a) Energy level diagram of the ^{85}Rb atom. (b) Dressed-state of Λ-type level systems. (c) Stokes and anti-Stokes ($\boldsymbol{E}_s$ and $\boldsymbol{E}_{as}$) produced by $\boldsymbol{E}_1$ and $\boldsymbol{E}_2$. (d) Shows division of FWM into horizontal ($\boldsymbol{E}_{Fp}$) and vertical ($\boldsymbol{E}_{Fs}$) signal through polarized beam splitter. (e) Schematic diagram of the experimental setup. Double headed arrows and filled dots denote the vertical polarization and horizontal polarization of incident beams (black lines with arrows), respectively.

signals of FWM processes can be modified by the dressing fields ($\boldsymbol{E}_1$ or/and $\boldsymbol{E}_2$). Therefore, by taking the dressing effects of $\boldsymbol{E}_1$ and $\boldsymbol{E}_2$ into account, Eq. (1) can be rewritten as

$$\rho_{31}^{(3)} = \frac{-iG_1G_2^*G_2'}{\left(d_{31} + G_2^2/d_{21} + G_1^2/\Gamma_{11}\right)^2\left[d_{21} + G_1^2/d_{23} + G_2^2/\Gamma_{22}\right]}, \tag{2}$$

where $d_{23} = \Gamma_{23} - i\Delta_2$. The polarized state of the dressing field $\boldsymbol{E}_2'$ is obtained by inserting a half-wave plate (HWP) (Fig. 1(e)). The polarized beam can be decomposed into linearly-polarized components while all other polarization fields are fixed. Therefore, Eq. (2) can be rewritten as

$$\rho_{xxyy}^{(3)} = \frac{iG_1G_2}{\left[d_{31} + \mu_x^2G_2^2\cos^2(2\theta)/d_{21} + G_1^2/\Gamma_{11}\right]^2} * \frac{G_2'\mu_x\cos(2\theta)}{\left[d_{21} + G_1^2/d_{23} + \mu_x^2G_2^2\cos^2(2\theta)/\Gamma_{22}\right]} \tag{3}$$

$$\rho_{yxyx}^{(3)} = \frac{iG_1G_2}{\left[d_{31} + \mu_y^2G_2^2\sin^2(2\theta)/d_{21} + G_1^2/\Gamma_{11}\right]^2} * \frac{G_2'\mu_y sin(2\theta)}{\left[d_{21} + G_1^2/d_{23} + \mu_y^2G_2^2\sin^2(2\theta)/\Gamma_{22}\right]} \tag{4}$$

The propagation equation of the FWM signals in the oven with Doppler effects is

$$I = I_F - I_A, \tag{5}$$

where $I_F = CN_F^2\mu^2\int_{v=-\infty}^{v=+\infty}(e^{-(v/u)^2}|\rho^{(3)}(v)|^2/u\sqrt{\pi})dv$ is the total intensity of the generated FWM signal. $\rho^{(3)}(v)$ is the density-matrix element of the FWM signal including pure FWM $\rho_{31}^{(3)}(v)$ and multi-dressed FWM signals. I_A is the absorption of the FWM signals in the medium and may be written as

$$I_A = I_F(1 - e^{-\alpha L}) = CN_F^2\mu^2\int_{v=-\infty}^{v=+\infty}(e^{-(v/u)^2}K\ \mathrm{Im}[F(v)]/u\sqrt{\pi})dv \tag{6}$$

where α is the absorption co-efficient. $K = I_0Lk_1/CN_F\hbar\varepsilon_0$ and $F = \hbar\varepsilon_0\chi/N_F\mu^2$ is the effective atom number and C is a constant.

μ is the dipole moment. v is the velocity of the atom due to Doppler effect and u is the most probable velocity. In the presence of I_A, the theory can well explain the interaction and propagation behaviors of the FWM signals.

3.1. Polarization controlled two FWM noise correlations

The second order intensity noises correlation function $G^{(2)}(\tau)$ between output fields (m and n) can be calculated by [15]

$$G^{(2)}_{mn}(\tau) = \frac{\langle \delta I_m(t)\delta I_n(t+\tau)\rangle}{\sqrt{\langle[\delta I_m(t)]^2\rangle\langle[\delta I_n(t+\tau)]^2\rangle}}\cos(\Delta\varphi). \tag{7}$$

For the weak coupling field FWM, the intensities of $\boldsymbol{E}_F$ are proportional to the $\rho^{(3)}_{31}$, where the brackets express the time average $\langle \delta I_i(t)\rangle = \int_t^{t+T}\delta I_i(t)/T$, $\langle I_i\rangle$ is the average intensity of each laser beam and $\delta I_i(t)$ gives the intensity fluctuations versus time. τ is time delay between the recorded signals, T is the time of integration. Moreover, we also observe the damping of Rabi oscillation [16], so that the oscillation and the decay terms as displayed could be added into the second-order correlation function $G^{(2)}_{mn}(\tau)[e^{-2\Gamma_+\tau}+e^{-2\Gamma_-\tau}-2\cos(\Omega_e\tau)e^{-(\Gamma_++\Gamma_-)\tau}]$, where, $\Gamma_+ = \Gamma_{10}$ and $\Gamma_- = \Gamma_{20}$ are natural linewidth without dressing fields. Further, the noise correlation can be controlled by the relative nonlinear phase induced by dressing beam. The nonlinear phase are determined by $\varphi_{m/n} = 2|(-i\omega_{m/n}/2c)\chi^{(3)}_{m/n}E_mE_n| * n_2I_2e^{-r^2}z/n_1$, where n_2 is nonlinear refractive index $n_2 = \mathrm{Re}\chi^{(3)}/(\varepsilon_0 c n_0)$, in which the third-order nonlinear susceptibility is given by $\chi^{(3)} = N\mu_F^2\mu_{i0}^2\rho^{(3)}_{j0}/\left(\hbar^3\varepsilon_0 G_F G_i^2\right)$ having atomic density N, ε_0 is permittivity of free space, and $\mu_F(\mu_{i0})$ is the dipole matrix element of the FWM transition. Hence, we can define $\Delta\varphi$ used in Eq. (7) as $\Delta\varphi = \varphi_m - \varphi_n$, which is responsible for switching correlation and squeezing through interaction of incident beams in Kerr medium by changing their power and polarization.

3.2. Two SP-FWM noise correlation

At the same time, we noticed that $\boldsymbol{E}_1$ and $\boldsymbol{E}_2$ produced Stokes ($\boldsymbol{E}_s$) and anti-Stokes ($\boldsymbol{E}_{as}$) (Fig. 1(b)). The process occurs in the subsystem ($|3\rangle - |1\rangle$) involving two beams $\boldsymbol{E}_1$ and $\boldsymbol{E}_2$. $\boldsymbol{E}_s$ and $\boldsymbol{E}_{as}$ satisfy the phase-matching condition. In nonlinear medium, $\chi^{(3)}$ is a function of the density-matrix elements which can be described by the perturbation chains $\rho^{(0)}_{11}\xrightarrow{k_1}\rho^{(1)}_{31}\xrightarrow{k_s}\rho^{(2)}_{21}\xrightarrow{k_2}\rho^{(3)}_{31(kas)}$, $\rho^{(0)}_{22}\xrightarrow{k_2}\rho^{(1)}_{32}\xrightarrow{k_{as}}\rho^{(2)}_{12}\xrightarrow{k_1}\rho^{(3)}_{31(ks)}$ and the corresponding density matrix elements for respective, $\boldsymbol{E}_s$ and $\boldsymbol{E}_{as}$ can be written as

$$\rho^{(3)}_{31as} = \frac{-iG_1G_sG_2}{(\Gamma_{31}+i\Delta_1)[\Gamma_{21}+i(\Delta_1-\Delta_2)](\Gamma_{31}+i\Delta_1)}, \tag{8}$$

$$\rho^{(3)}_{32s} = \frac{-iG_2G_{as}G_1}{(\Gamma_{31}+i\Delta_2)[\Gamma_{12}+i(\Delta_2-\Delta_1)](\Gamma_{32}+i\Delta_2)}, \tag{9}$$

For the weak coupling fields of Stocks and anti-Stokes, the intensities of $\boldsymbol{E}_s$ and $\boldsymbol{E}_{as}$ are proportional to the numbers of photons $\langle\hat{a}^\dagger\hat{a}\rangle$ and $\langle\hat{b}^\dagger\hat{b}\rangle$, respectively. When $\boldsymbol{E}_{s/as}$ fields propagate through the medium, then they can be evolved under the Hamiltonian of the system. The measured photon numbers at two output channels are

$$\langle\hat{a}^\dagger\hat{a}\rangle = \{\cosh[2t\sqrt{G}\cos\varphi] - \cos[2t\sqrt{G}\sin\varphi]\}g_s/2g_{as}, \tag{10}$$

$$\langle\hat{b}^\dagger\hat{b}\rangle = \{\cosh[2t\sqrt{G}\cos\varphi] - \cos[2t\sqrt{G}\sin\varphi]\}g_{as}/2g_s, \tag{11}$$

where $G = g_sg_{as}$, $\varphi = (\varphi_s+\varphi_{as})/2$, φ_s and φ_{as} are phase angles of $\boldsymbol{E}_s$ and $\boldsymbol{E}_{as}$, respectively. As a result, the correlation function between $\boldsymbol{E}_s$ and $\boldsymbol{E}_{as}$ can be expressed as

$$G^{(2)}_{as-s}(\tau) = \frac{\langle \delta I_{as}(t)\delta I_s(t+\tau)\rangle}{\sqrt{\langle[\delta I_{as}(t)]^2\rangle\langle[\delta I_s(t+\tau)]^2\rangle}}\cos(\Delta\varphi) = \frac{A}{\sqrt{BCDE}}\cos(\Delta\varphi), \tag{12}$$

where $A = R_1|\int d\omega_{as}e^{-i\omega_{as}\tau}\cosh(gL)\sinh(gL)|^2$, $B = R_2\int d\omega_s\sinh^2(gL)$, $C = R_3\int d\omega_{as}\sinh^2(gL)$, $D = R_4\int d\omega_s\cosh^2(gL)$, $E = R_5\int d\omega_{as}\cosh(gL)^2$, where $R_1 = |R_sR_{as}\boldsymbol{E}_s\boldsymbol{E}_{as}|^2$, $R_{2,4} = R_s|\boldsymbol{E}_s|^2$, $R_{3,5} = R_{as}|\boldsymbol{E}_{as}|^2$, $R_{as/s} = V/[(2\pi)^3v_{as/s}]$, $\boldsymbol{E}_{as/s} = \hbar_{as/s}/2V)^{1/2}$. V is the quantization volume. Considering the influence of Stocks and anti-Stokes fields, we have lower decay rate and higher lifetime, this is due to broad band laser source excitation. The shape of the correlation peak for Stokes and anti-Stokes can be determine by the parameter of correlation function which can be written as $A = R_1|A_1|^2[e^{-(2\Gamma_++\zeta)|\tau|}+e^{-(2\Gamma_-+\zeta)|\tau|}-2\cos(\Omega_e|\tau|)e^{-(\Gamma_++\Gamma_-+\zeta)|\tau|}]$. Here A is related with τ only. $A_1 = A_2\mathrm{N}(\mu_{10}\mu_{20}E_1)^2\varpi_{as}L/(2c\varepsilon_0\hbar^3)$, and Ω_e is the Rabi oscillation. Where, $\Gamma_+ = \Gamma_{10}$ and $\Gamma_- = \Gamma_{20}$ are natural linewidth, ζ is linewidth of $\boldsymbol{E}_s$ and $\boldsymbol{E}_{as}$, $\Omega_e = |\Delta_1|$. If we only consider the influence of FWM, we have higher decay rate and reduced lifetime, which results in broad peak correlation structure, caused by narrow band laser source and destructive dressing effect (G_1 and G_2) at resonance ($\Delta_2 = 0$) and nearby points. The parameter A for FWM can be expressed as

$$A = R_1|A_1|^2[e^{-2\Gamma_+|\tau|}+e^{-2\Gamma_-|\tau|}-2\cos(\Omega_e|\tau|)e^{-(\Gamma_++\Gamma_-)|\tau|}].$$

3.3. Two FWM intensity-difference squeezing

The degree of two-mode intensity-difference squeezing [13,14] between output beams $\boldsymbol{E}_{Fs}$ and $\boldsymbol{E}_{Fp}$ can be given by

$$Sq = \mathrm{Log}_{10}\left[\frac{\langle\delta^2(\hat{I}_m-\hat{I}_n)\rangle}{\langle\delta^2(\hat{I}_m+\hat{I}_n)\rangle}\right]\cos(\Delta\varphi) \approx \mathrm{Log}_{10}\left[\frac{\langle\delta^2(\hat{N}_m-\hat{N}_n)\rangle}{\langle\delta^2(\hat{N}_m+\hat{N}_n)\rangle}\right]\cos(\Delta\varphi) = -2\mathrm{Log}_{10}(2G-1)cos(\Delta\varphi), \tag{13}$$

where $\langle\delta^2(\hat{N}_m-\hat{N}_n)\rangle$ is the mean square deviation of the intensity difference and $\langle\delta^2(\hat{N}_m+\hat{N}_n)\rangle$ is the mean square deviation of the intensity sum.

4. Experimental results and discussions

In order to understand the interaction between horizontal and vertical components of FWM signal and the AT splitting, from the designed experiments, we have taken the following results. There exist one Λ-type EIT window (satisfying $\Delta_1-\Delta_2 = 0$ condition) and the FWM signal ($\boldsymbol{E}_F$). Fig. 2(a)–(c) show that the intensity of the two FWM signals are moved position by scanning $\boldsymbol{k}_2$. Fig. 2 (d)–(f) show that the polarization states of dressing fields $\boldsymbol{E}_2'$ as externally controlled variables.

Next, we focus on the AT splitting of the FWM signal within the EIT window. When the coupling field $\boldsymbol{E}_2$ is incident, these fields ($\boldsymbol{E}_2$ ($\boldsymbol{E}_2'$) and $\boldsymbol{E}_1$) can dress the energy level $|3\rangle$ together. $\boldsymbol{E}_1$ first creates the primary dressed states $|G_{1\pm}\rangle$, then $\boldsymbol{E}_2$ creates the secondary dressed states $|G_{1+\pm}\rangle$ at a proper frequency detuning (tuned to near either the upper or lower dressed state $|G_{1+}\rangle$ or $|G_{1-}\rangle$, as shown in Fig. 1(b). This generates the secondary AT splitting for the FWM signal and the appearance of three peaks in Fig. 2(a–c), respectively. If we set $|1\rangle$ as the frequency reference point, the Hamiltonian for primary energy can be written as:

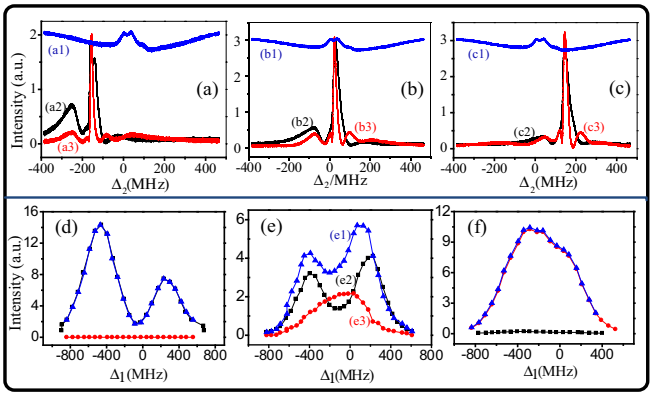

Fig. 2. (a)–(c) Measured the two FWM signal intensities at different detuning −200, 0 and 200 MHz, respectively. (a1) Saturated absorption spectrum of rubidium atom (SAS). (a2) The vertical component of FWM (I_S). (a3) The horizontal component of FWM (I_P). (d)–(f) Polarization dependence of the suppressed FWM signals. Variations of total intensity I_T (e1), I_S (e2) and I_P (e3) at different angle θ = 0°, 22.5° and 45° in (d)–(f), respectively. $\boldsymbol{E}_1$ = 3.9 mW, $\boldsymbol{E}_2$ = 10 mW, $\boldsymbol{E}'_2$ = 7.2 mW.

$H = -\hbar\begin{bmatrix} 0 & G_1 \\ G_1^* & (-1)^i\Delta_1 \end{bmatrix}$, from the equation $H|G_{1\pm}\rangle = \lambda_\pm|G_{1\pm}\rangle$, we can obtain $\lambda_\pm = [(-1)^i\Delta_1 \pm \sqrt{\Delta_1^2 + 4|G_1|^2}]/2$. In addition, $\boldsymbol{E}_2$ splits $|G_{1+}\rangle$ into $|G_{1+\pm}\rangle$ if $\Delta_2 > 0$, or splits $|G_{1-}\rangle$ into $|G_{1-\pm}\rangle$ if $\Delta_2 < 0$. The Hamiltonian for secondary energy can be written as $H' = -\hbar\begin{bmatrix} \Delta_i & G_2 \\ G_2^* & 0 \end{bmatrix}$, where $\Delta_i = \Delta_2 - (-1)/\lambda_\pm$. From the relation $H'|G_{1\pm\pm}\rangle = \lambda_{\pm\pm}|G_{1\pm\pm}\rangle$, we can obtain $\lambda_{\pm\pm} = [(-1)^j\Delta_i \pm \sqrt{\Delta_i^2 + 4|G_2|^2}]/2$. We can obtain the expression splitting distance between $|G_{1++}\rangle$ and $|G_{1-}\rangle$ as $\Delta = 2\sqrt{|G_1|^2 + |G_2|^2}$, provided $\Delta_1 = \Delta_2 = 0$, with the detuning factors of Δ_2 as −155 MHz, 26 MHz and 146 MHz, respectively. The three peaks, from left to right, correspond to the primary $|G_{1-}\rangle$ (satisfying $\Delta_1 = \lambda_-$), secondary, $|G_{1++}\rangle$ (satisfying $\Delta_1 = \lambda_{++}$) and tertiary $|G_{1+-}\rangle$ dressed state (satisfying $\Delta_1 = \lambda_{+-}$), respectively (Fig. 1(b)). Three AT splitting are not evenly distributed on both sides of resonance point due to many hyperfine energy levels of ^{85}Rb. When $\boldsymbol{k}_1$ changed (Δ_1 from −800 MHz to 400 MHz) the FWM background signal come from two-photon resonance signal dressed by G_1, all point satisfy $\Delta_1 - \Delta_2 = 0$, near the zero point ($\Delta_1 \approx 0$, $\Delta_2 \approx 0$). Since the dressing effect are stronger, so we can see two peaks, the left peak $\Delta_1 = -462$ MHz, the right peak $\Delta_1 = 242$ MHz, correspondingly one dark state at $\Delta_1 = -66$ MHz in Fig. 2(d), and two bright states $\Delta_1 = -399$ MHz, $\Delta_1 = 242$ MHz and one dark state $\Delta_1 = -110$ MHz in Fig. 2(e).

Next, we consider FWM processes effectively controlled by the polarized multi-dark-state. Specifically, AT splitting of FWM can be modulated [17] by inserting HWP of the involved laser beam $\boldsymbol{E}'_2$ as shown in Fig. 1(e). The Hamiltonian of the double-Λ type three-level system can be written as the matrix:

$$H = \hbar[\Delta_1|3\rangle\langle 3| + (\Delta_1 - \Delta_2)|2\rangle\langle 2|] + \hbar(G_1|1\rangle\langle 3| - G_2|3\rangle\langle 2| + G'_2|2\rangle\langle 3|). \quad (14)$$

Under the resonant conditions of $\Delta_1 - \Delta_2 = 0$, $\Delta_1 = 0$ and $\Delta_2 = 0$, we can get two easily identified dark states:

$$|D1\rangle = \frac{G_2|1\rangle - G_1|2\rangle}{\sqrt{|G_1|^2 + |G_2|^2}} \approx |1\rangle - \frac{G_1}{G_2}|2\rangle,$$
$$|D2\rangle = \frac{G'_2|1\rangle - G_1|2\rangle}{\sqrt{|G_1|^2 + |G'_2|^2}} \approx |1\rangle - \frac{G_1}{G'_2}|2\rangle. \quad (15)$$

The total dark state amplitude is then given by

$$|D\rangle = |D1\rangle + |D2\rangle = 2|1\rangle - (G_1/G_2 + G_1/G'_2). \quad (16)$$

We want to see how the populations of the atoms in the dark states vary as the four uncoupled states interfere with each other. That is, we would like to find $|\langle D|\psi\rangle|^2$. The wave function of the atom in its bare-state basis is written as $|\psi\rangle = c_0|1\rangle + c_1|2\rangle + c_2|3\rangle$ the intensity of FWM signal is $I = |N'\mu\rho_{31}^{(3)}|^2$, where $N' = N(1 - |\langle D|\psi\rangle|^2)$. In order to quantitatively compare with the observed changes of the FWM signal peaks as $\boldsymbol{E}'_2$ polarization changes, the area of the spectrum under the peak and the height of each peak are investigated. The changes of the FWM spectrum is well described by the function $\cos^2 2\theta$, θ is the rotated angles of the HWP, each peak of the FWM process will be controlled by polarization property [18]. Fig. 2(d)–(f) show that as the polarization angle θ changed from 0° to 22.5° and then to 45°, the total FWM changed from two peaks to one peak. In Fig. 2(d), when $\theta = 0°$ one can find that the trend of evolution in the relative height of the left peak and the right peak is opposite, the left peak is higher than the right peak. Fig. 2(e) depicts that the intensity of the horizontal component ($\boldsymbol{E}_{Fp}$) and vertical component ($\boldsymbol{E}_{Fs}$) of the FWM changed by polarization angle θ of $\boldsymbol{E}'_2$. $\boldsymbol{E}_{Fs}$ splits into two peaks, the right peak is higher than the left peak. However, $\boldsymbol{E}_{Fp}$ does not split at 22.5°, this is because dressed effect of the vertical component also increases with increasing angle of $\boldsymbol{E}'_2$, different from the horizontal component which is dressed-insensitive. Changing detuning Δ_1 of $\boldsymbol{E}_1$ will influence dressing effect, because of $\mu_y > \mu_x$, in Eqs. (3) and (4) as $\mu_y^2 G_2^2 \sin^2(2\theta)/d_{21} > \mu_x^2 G_2^2 \cos^2(2\theta)/d_{21}$. In Fig. 2(f), experimental condition is similar to Fig. 2(e) except for polarization angle $\theta = 45°$, where one can find that $\boldsymbol{E}_{Fs} = 0$ and $\boldsymbol{E}_{Fp}$ has no splitting.

4.1. Correlation or anti-correlation

Next, we focus on the intensity noise correlation between the output beams $\boldsymbol{E}_{Fs}$ and $\boldsymbol{E}_{Fp}$ as well as between Stokes ($\boldsymbol{E}_s$) and anti-Stokes ($\boldsymbol{E}_{as}$) as shown in Fig. 3. Fig. 3(a) shows to ensure the two components of FWM intensity are always equal at different detuning points, we change the polarization of $\boldsymbol{E}'_2$. Fig. 3(b) shows the two-stage line shape of correlation, including the sharp peak (solid curve) between stokes and anti-Stokes (Eq. (12), and the broad peak correlation (dash curve) between two components ($\boldsymbol{E}_{Fs}$ and $\boldsymbol{E}_{Fp}$) of coherent FWMs (Eq. (7)). This is because stokes and anti-Stokes have lower decay rate and higher lifetime, this is also due to broad band laser source excitation, and two components ($\boldsymbol{E}_{Fs}$ and $\boldsymbol{E}_{Fp}$) of coherent FWMs have higher decay rate and reduced lifetime $\Gamma >> \zeta$, which results out to be broad peak correlation structure, it is also due to narrow band laser source and destructive dressing effect (G_1 and G_2) at resonance ($\Delta_2 = 0$) and nearby points.

In Fig. 3(c), by adjusting two polarized components of the FWM with equal intensity when $\Delta_1 = 0$, and $\boldsymbol{E}'_{2s}$ = 5.7 mW, $\boldsymbol{E}'_2$ = 8.8 mW, $\boldsymbol{E}_1$ = 3.9 mW, $\boldsymbol{E}_2$ = 12.1 mW. During the experiment, all parameters are fixed except detuning is changed from −400 to 800 MHz. In Fig. 3(d), experimental conditions are the same as defined in Fig. 3(c) but changes the power of input fields, $\boldsymbol{E}'_{2s}$ = 2.55 mW, $\boldsymbol{E}'_{2p}$ = 3.47 mW, $\boldsymbol{E}'_2$ = 7.02 mW, $\boldsymbol{E}_1$ = 3.9 mW and $\boldsymbol{E}_2$ = 10 mW. In Fig. 3(e), in order to get the equal intensity of two different polarized output components of FWM signal at the different detuning conditions, we use HWP to change the polarization state of $\boldsymbol{E}'_2$ (7.2 mW), and $\boldsymbol{E}_1$ = 3.9 mW, $\boldsymbol{E}_2$ = 10 mW. From Fig. 3(c)–(e), we can see the correlation switched from negative to positive. Meanwhile the broad peak amplitude of correlation values decreases from left to right and sharp peak amplitude increase and finally

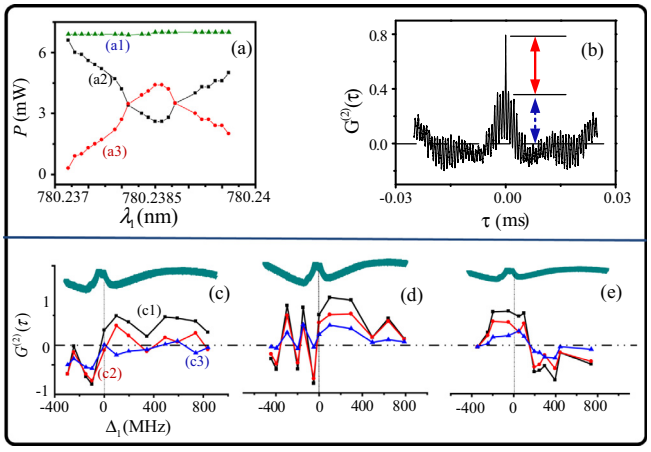

Fig. 3. Measured intensity and intensity noise correlation between signal from APD1 and APD2 (a1)–(a3) Measured total power, horizontal component power and vertical component power of $\boldsymbol{E}_2'$, respectively. (b) Measured intensity noise correlation between $\boldsymbol{E}_{Fs}$ and $\boldsymbol{E}_{Fp}$ also between Stokes ($\boldsymbol{E}_s$) and anti-Stokes ($\boldsymbol{E}_{as}$). The solid curve represents the sharp peak correlation, the dash curve represents the broad peak correlation. (c)–(e) Frequency detuning and polarization dependences of the maximum correlation value $G^{(2)}(0)$. (c1)–(c3) Frequency detuning dependences of the sharp peak, the broad peak correlation and total correlation, respectively.

decrease as shown in broad peak and sharp peak amplitude dependence.

In this section, we discuss the correlation and anti-correlation existing in our experiment with theoretical explanation of switching phenomenon. The noise correlation can be controlled by the initial phase and relative nonlinear phase. Firstly, we consider the noise correlation influenced by the initial phase. To explain this phenomenon, we introduce populations into corresponding density matrix elements. When the pumping effect of $\boldsymbol{E}_2$ is considered, the lasers $\boldsymbol{E}_1$ and $\boldsymbol{E}_2$ do not satisfy two-photon resonance, the initial populations of the ground states $(|1\rangle, |2\rangle)$ are:

$$\rho_{11}^{(0)} = \frac{\Omega_2^2}{\Omega_1^2+\Omega_2^2} - f(t), \quad \rho_{22}^{(0)} = \frac{\Omega_1^2}{\Omega_1^2+\Omega_2^2} + f(t), \tag{17}$$

where $f(t)$ can be viewed as the population fluctuation with a real value. Moreover, the far smaller ratio between the Rabi frequencies (generated fields) and their detuning will nullify the mutual coupling among these fields. For the probe transmission and FWM signals, the propagation equations are given by $\frac{\partial G_{Fp}}{\partial z} = i\eta\rho_{31Fp}^{(1)}, \frac{\partial G_{Fs}}{\partial z} = i\eta\rho_{31Fs}^{(1)}$, where $\eta = 3\lambda^2 N\Gamma_{10}/8\pi$, N is the atomic density, λ is the resonant wavelength of D_1 line, and G_{Fp} & G_{Fs} are Rabi frequencies of E_{Fs} & E_{Fp}, respectively. If $\eta L << \Gamma_{31}$ we can get $G_{Fp}^{out}(t) \approx G_{Fp} + i\eta L\rho_{31Fp}^{(1)}(t)$, $G_{Fs}^{out}(t) \approx G_{Fs} + i\eta L\rho_{31Fs}^{(1)}(t)$.

Transmission intensity can be expressed as

$$I_{Fp}(t) \approx G_{Fp}^2 - 2G_{Fp}\eta L\ \mathrm{Im}[\rho_{31Fp}^{(1)}(t)],$$
$$I_{Fs}(t) \approx G_{Fs}^2 - 2G_{Fs}\eta L\ \mathrm{Im}[\rho_{31Fs}^{(1)}(t)]$$

the intensity fluctuation can be described as $\delta I_{Fp}(t) = G_{Fp}\eta L\ \mathrm{Im}\left[\delta\rho_{31Fp}^{(1)}(t)\right], \delta I_{Fs}(t) = G_{Fs}\eta L\ \mathrm{Im}\left[\delta\rho_{31Fs}^{(1)}(t)\right]$. So, the intensity noise correlation function $G^{(2)}(\tau)$ between any these two fields (E_{Fs} and E_{Fp}) can be calculated as

$$G_{Fp-Fs}^{(2)}(\tau) = \frac{\langle\delta I_{Fp}(t)\delta I_{Fs}(t+\tau)\rangle}{\sqrt{\langle[\delta I_{Fp}(t)]^2\rangle\langle[\delta I_{Fs}(t+\tau)]^2\rangle}} = \frac{\left\langle \mathrm{Im}\left[\delta\rho_{31Fp}^{(1)}(t)\right]\mathrm{Im}\left[\delta\rho_{31Fs}^{(1)}(t+\tau)\right]\right\rangle}{\sqrt{\left\langle\left\{\mathrm{Im}\left[\delta\rho_{31Fp}^{(1)}(t)\right]\right\}^2\right\rangle\left\langle\left\{\mathrm{Im}\left[\delta\rho_{31Fs}^{(1)}(t+\tau)\right]\right\}^2\right\rangle}} \tag{18}$$

The sign of correlation depends on these two fields corresponding to their first-order matrix elements of the fluctuation of the imaginary part. If the same signs, the correlation is a positive; On the contrary, if the symbol is negative, the correlation is negative. We get

$$\mathrm{Im}\left[\delta\rho_{31Fp}^{(1)}\right] = \frac{G_{Fp}\Gamma_{31}\delta\rho_{11}^{(0)} + G_2\Gamma_{32}\delta\rho_{21}^{(0)}}{\Delta_1^2+\Gamma_{31}^2},$$
$$\mathrm{Im}\left[\rho_{31Fs}^{(1)}\right] = \frac{G_{Fs}\Gamma_{31}\delta\rho_{11}^{(0)} + G_2\Gamma_{32}\delta\rho_{21}^{(0)}}{\Delta_1^2+\Gamma_{31}^2}. \tag{19}$$

The fluctuation of the population of level $|1\rangle$ is $\delta\rho_{11}^{(0)}(t) = -f(t)$, and then based on the simplified matrix elements, the intensity fluctuations of the two signals are: $\mathrm{Im}\left[\delta\rho_{31Fp}^{(1)}\right] = -\frac{G_{Fp}\Gamma_{31}f(t)}{\Delta_1^2+\Gamma_{31}^2}, \mathrm{Im}\left[\rho_{31Fs}^{(1)}\right] = -\frac{G_{Fs}\Gamma_{31}f(t)}{\Delta_1^2+\Gamma_{31}^2}$. Then, by inserting Eq. (19) into Eq. (18), one can obtain the intensity noise correlations as:

$$G_{Fp-Fs}^{(2)}(\tau) = \frac{\left\langle \mathrm{Im}\left[\delta\rho_{31Fp}^{(1)}(t)\right]\mathrm{Im}\left[\delta\rho_{31Fs}^{(1)}(t+\tau)\right]\right\rangle}{\sqrt{\left\langle\left\{\mathrm{Im}\left[\delta\rho_{31Fp}^{(1)}(t)\right]\right\}^2\right\rangle\left\langle\left\{\mathrm{Im}\left[\delta\rho_{31Fs}^{(1)}(t+\tau)\right]\right\}^2\right\rangle}} = \frac{\langle f(t)f(t+\tau)\rangle}{\sqrt{\langle[f(t)]^2\rangle\langle[f(t+\tau)]^2\rangle}}. \tag{20}$$

In Eq. (20) we always get positive value of noise correlation of two mode polarized FWM (initial phase $\Delta\varphi = 0$ ($\Delta\varphi = \varphi_m - \varphi_n$)), while from experiment result (Fig. 3(c)–(e)) we can see the noise correlation have both positive and negative. Considering the noise correlation can be controlled by the relative nonlinear phase $\Delta\varphi$, the correlation function in Eqs. (7) and (12) is multiplied by $\cos(\Delta\varphi)$ factor. By changing the detuning, power and polarization of probe, pump and dressing fields, the switching is achieved due to interaction among these dressing fields. When we change the detuning of $\boldsymbol{k}_1$, the FWM signal is dressed by G_1, the intensity spectrum of FWM split into two bright states $\Delta_1 = -399$ MHz, $\Delta_1 = 242$ MHz and one dark state $\Delta_1 = -110$ MHz (Fig. 2(c)). Corresponding to the primary $|G_{1-}\rangle$ (satisfying $\Delta_1 = \lambda_-$), secondary $|G_{1++}\rangle$ (satisfying $\Delta_1 = \lambda_{++}$) $|G_{1+-}\rangle$ (satisfying $\Delta_1 = \lambda_{+-}$), respectively (Fig. 1(b)). Correlation $G^{(2)}(\tau)$ are switched from negative to positive, only by changing detuning of $\boldsymbol{E}_1$ due to its dressing effect as shown in Fig. 3(c) and (d). In Fig. 3(c) $\boldsymbol{E}_2'$ has fixed polarization angle, $\boldsymbol{E}_1$ and $\boldsymbol{E}_2$ power are constant. These results may be explained by nonlinear refractive index of Kerr medium. Since the dressing state created by $\boldsymbol{E}_2'$ can modulate the nonlinear refractive index, such modulation effect is governed by self-phase modulated (SPM) and cross-phase modulated (XPM) in Kerr nonlinear medium, the relative nonlinear phase between two FWM signals $\Delta\varphi = \Delta\varphi_1 + \Delta\varphi_2$ is significantly modulated, here $\Delta\varphi_1 = 2(|E_m|^2 n_2^m - |E_n|^2 n_2^n)\zeta e^{-r^2} z/n_1$, $\Delta\varphi_2 = 2(k_m n_2^m - k_n n_2^n)|E_2'|^2 \cos\theta(e^{-r^2}z)/n_1\zeta = |G_2/G_1|^2$, m and n represents the horizontal component and the vertical components of FWM. When detuning factor Δ_1 from −400 to 800 MHz, the vertical component of FWM spectrum splits into two peaks, the left peak higher than the right peak (Fig. 2(d)). When Δ_1 changed from 0 to −400 MHz $|E_{Fs}|^2 n_2^{Fs} > |E_{Fp}|^2 n_2^{Fp}$, the relative nonlinear phase $\Delta\varphi_1$ gradually changed from $\pi/2$ to π, corresponding noise correlation are negative; Δ_1 changed from 0 MHz to 800 MHz $|E_{Fs}|^2 n_2^{Fs} < |E_{Fp}|^2 n_2^{Fp}$, the relative nonlinear phase $\Delta\varphi_1$ gradually changed from 0 to $\pi/2$, corresponding noise correlation are positive (Eq. (7)). Because we only changed the detuning Δ_1, modulation effect governed by XPM is slight $\Delta\varphi_2 = 0$. In Fig. 3(d), set of experimental conditions are same with Fig. 3(c) but the power of $\boldsymbol{E}_2$ is changed from 12.1 to 10mW, while powers of $\boldsymbol{E}_2'$ are changed from 8.8 to 7.02 mW. Because of dressing fields power changed, the power

difference of dressing fields G_1 and G_2 become smaller, double dressing effect affect the FWM intensity fluctuations (Eqs. (3) and (4)) as a result in noise correlation switching. When $\Delta_1 = -295$ MHz and $\Delta_1 = -147$ MHz, noise correlations are positive. With detuning Δ_1 changing from -400 to 800 MHz, the same nonlinear phase $\Delta\varphi_1$ change with Fig. 3(c), corresponding noise correlation from negative to positive accompanied by strong oscillation. In Fig. 3(e), we find the amplitude of correlation peak at delay time $\tau = 0$ is switched from positive (0.934) to negative (-0.885) showing that switching of correlation into anti-correlation. When detuning factor Δ_1 changes from 0 to -400 MHz, the relative nonlinear phase $\Delta\varphi_1$ gradually changed from $\pi/2$ to π; Δ_1 changed from 0 to 800 MHz, the relative nonlinear phase $\Delta\varphi_1$ gradually changed from 0 to $\pi/2$. At the same time the modulation of the nonlinear phase can be realized not only by changing the detuning of $\boldsymbol{E}_1$, but also by changing the polarization of $\boldsymbol{E}_2'$ as well. Modulated polarization can be achieved by incident HWP as shown in Fig. 1(e) in front of incident beam $\boldsymbol{E}_2'$. One can find similar behavior with the detuning dependence, where the intensity fluctuations are changed from correlated to anti-correlated as polarized modulation from different polarization states. This phenomenon can be interpreted by the XPM, where the relative nonlinear phase $\Delta\varphi_2$. With the change of polarization angle, $\Delta\varphi_2$ gradually changed from $3\pi/2$ to π. Therefore, when Δ_1 changes from 0 to -400 MHz, the total nonlinear phase $\Delta\varphi = \Delta\varphi_1 + \Delta\varphi_2$ gradually changed from $3\pi/2$ to 2π; Δ_1 changed from 0 MHz to 800 MHz, the total nonlinear phase $\Delta\varphi$ gradually changed from π to $3\pi/2$. Corresponding noise correlation switched from positive to negative, accompanied by a slight oscillation.

4.2. The intensity-difference squeezing

In this section, we analyzed the degree of intensity difference squeezing between output beams $\boldsymbol{E}_{Fs}$ and $\boldsymbol{E}_{Fp}$, and their corresponding degree of squeezing is shown in Fig. 4(a–c). Fig. 4(a)–(c) corresponds to Fig. 3(c)–(e), the noise correlation and the intensity-difference squeezing are calculated using the same experimental data. We have also compared the noise correlation and the intensity-difference squeezing (Fig. 4(c) and (d)).

Like correlation result, by substituting $\delta I_{m,n}(t)$ into Eq. (13), the influence of the relative nonlinear phase on intensity fluctuations squeezing are also investigated. Fig. 4(a)–(c) demonstrated that the intensity-difference signal (black curve) can be switched to higher or lower than the total noise signal (red curve)[1] by changing $\Delta\varphi = \pi$ to 0 respectively, which is corresponding to anti-squeezing to squeezing. It is worth mentioning that the variation tendencies of the intensity fluctuations squeezing and the corresponding intensity fluctuations correlation are in accordance with each other. The intensity-difference squeezing shows same behavior with noise correlation. When we change the detuning of Δ_1, the noise correlation and the intensity-difference squeezing can be controlled by dark states and bright states, from left to right, correspond to the primary $|G_{1-}\rangle$ (satisfying $\Delta_1 = \lambda_-$), secondary $|G_{1++}\rangle$ (satisfying $\Delta_1 = \lambda_{++}$) and tertiary dressed states $|G_{2+-}\rangle$ (satisfying $\Delta_1 = \lambda_{+-}$), respectively (Fig. 1(b)). As detuning Δ_1 changed from -400 to 800 MHz, make the nonlinear phase $\Delta\varphi$ gradually changed from π to 0, the squeezing switched from anti-squeezing to squeezing as shown in Fig. 4(a). Since, experimental conditions of Fig. 4(b) are same with Fig. 4(a) but the powers of $\boldsymbol{E}_2$ are changed from 12.1 mW to 10 mW, while $\boldsymbol{E}_2'$ from 8.8 mW to 7.02 mW, the results obtained are substantially similar. As detuning Δ_1 and HWP angle changing, make the nonlinear phase $\Delta\varphi$ gradually changed from π to 2π (Eq. (13)), we can get the intensity-difference squeezing switched from squeezing to anti-squeezing as shown in Fig. 4(c). Compared with Fig. 4 (c) and (d), we compare and analyze the nonlinear phase modulated correlation and the intensity-difference squeezing, the correlation and squeezing can be switched into anti-correlation and anti-squeezing and in the correlation obvious region squeezing phenomenon is more obvious. Physically this phenomenon occurs due to the rubidium atoms near the resonance frequency of FWM efficiency is enhanced, the output signal intensity is bigger but its noise is almost the same.

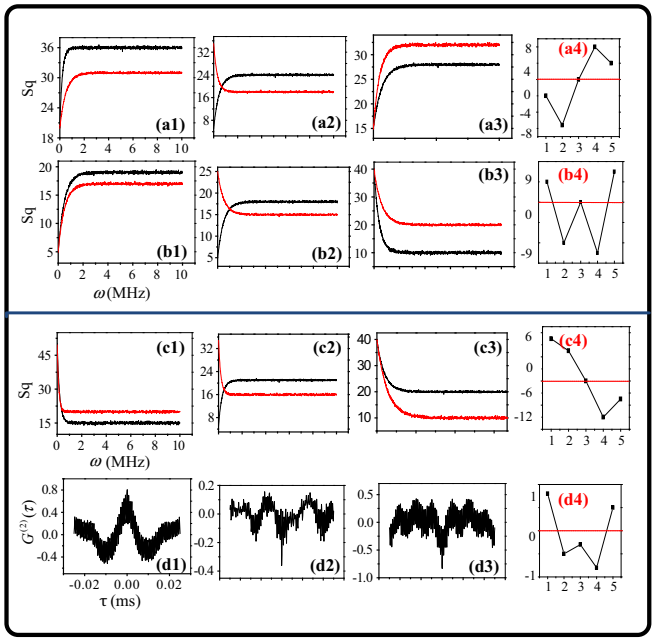

Fig. 4. (a1)–(b3) Measured intensity-difference squeezing between output beams $\boldsymbol{E}_{Fs}$ and $\boldsymbol{E}_{Fp}$, all experimental conditions are identical with each other except for their spectral positions Δ_1 of a1 ($\Delta_1 = -350$ MHz), a2 ($\Delta_1 = 0$ MHz), a3 ($\Delta_1 = 500$ MHz) respectively. (b1)–(b4) are similar to (a1)–(b4), except for input power of $\boldsymbol{E}_2$, which is changed from 12.1 mW to 10 mW and $\boldsymbol{E}_2'$ from 8.8 mW to 7.02 mW. (a4) and (b4) Show the dependences of amount of squeezing at the analysis frequency corresponding to (a1)–(a3) and (b1)–(b3), respectively. (c)–(d) Measured intensity-difference squeezing and intensity noise correlation between output beams $\boldsymbol{E}_{Fs}$ and $\boldsymbol{E}_{Fp}$, all experimental conditions are identical except for their spectral positions Δ_1 and polarization state of the dressing field $\boldsymbol{E}_2'$, c1, d1 ($\Delta_1 = -350$ MHz, $\theta = 0°$) c2, d2 ($\Delta_1 = 0$ MHz, $\theta = 22.5°$) c3, d3 ($\Delta_1 = 500$ MHz, $\theta = 45°$). (d4) Frequency detuning and polarization dependences of the maximum correlation value $G^{(2)}(0)$.

5. Conclusion

We have observed FWM processes in a double-Λ level of rubidium atomic system with EIT windows. We find that the efficiency of resonant FWM process is much higher efficiency than the off-resonant and the AT splitting of FWM induced by the generated fields is observed. Meanwhile, the dressed noise correlation and intensity-difference squeezing based on FWM process in rubidium vapor have been observed experimentally and explained theoretically. And the two-stage line shape of correlation that exhibits a sharp peak and a broad peak is also studied. The sharp peak and the broad peak are from the correlation of two spontaneous parametric FWMs and that of the vertical component and horizontal component of two coherent FWMs. When the correlation is positive we have positive squeezing, when the correlation is negative we get anti-squeezing. We explained that the correlation and squeezing can be switched by controlling the detuning and polarization of the dressing fields which determine the relative initial

[1] For interpretation of color in Fig. 4, the reader is referred to the web version of this article.

phase and nonlinear phase. These results are attributed to dressing-induced nonlinear phase. Such researches can find potential applications in all-optical communication and optical information processing on photonic chips.

Acknowledgements

This work was supported by the 973 Program (2012CB921804), KSTIT of Shaanxi Province (2014KCT-10), NSFC (11474228, 61308015, and 61205112).

References

[1] S.E. Harris, Electromagnetically induced transparency, Phys. Today 50 (1997) 36.
[2] M. Fleischhauer, A. Imamoglu, J.P. Marangos, Electromagnetically induced transparency: optics in coherent media, Rev. Mod. Phys. 77 (2005) 633.
[3] Y.Q. Zhang, Z.K. Wu, M.R. Belic, H.B. Zheng, Z.G. Wang, Min Xiao, Yanpeng Zhang, Laser Photon. Rev. 9 (2015) 331.
[4] L.M. Duan, M.D. Lukin, J.I. Cirac, P. Zoller, Long-distance quantum communication with atomic ensembles and linear optics, Nature 414 (2001) 413.
[5] M. Xiao, Y.Q. Li, S.Z. Jin, J. Gea-Banacloche, Measurement of dispersive properties of electromagnetically induced transparency in rubidium atoms, Phys. Rev. Lett. 74 (1995) 666–669.
[6] J. Gea-Banacloche, Y.Q. Li, S.Z. Jin, M. Xiao, Electromagnetically induced transparency in ladder-type inhomogeneously broadened media: theory and experiment, Phys. Rev. A 51 (1995) 576–584.
[7] P. Hemmer, D. Katz, J. Donoghue, M. Cronin-Golomb, M. Shahriar, P. Kumar, Efficient low-intensity optical phase conjugation based on coherent population trapping in sodium, Opt. Lett. 20 (1995) 982.
[8] Y.G. Du, Y.P. Zhang, C.C. Zuo, C.B. Li, Z.Q. Nie, H.B. Zheng, M.Z. Shi, R.M. Wang, J. P. Song, K.Q. Lu, M. Xiao, Controlling four-wave mixing and six-wave mixing in a multi-Zeeman-sublevel atomic system with electromagnetically induced transparency, Phys. Rev. A 79 (2009) 063839.
[9] B. Wang, S.J. Li, J. Ma, H. Wang, K.C. Peng, M. Xiao, Controlling the polarization rotation of an optical field via asymmetry in electromagnetically induced transparency, Phys. Rev. A 73 (2006) 051801.
[10] Y.C. Chen, C.W. Lin, I.A. Yu, Role of degenerate Zeeman levels in electromagnetically induced transparency, Phys. Rev. A 61 (2000) 053805.
[11] V.A. Sautenkov, Yu V. Rostovtsev, M.O. Scully, Switching between photon-photon correlations and Raman anticorrelations in a coherently prepared Rb vapor, Phys. Rev. A 72 (2005) 065801.
[12] H.B. Zheng, U. Khadka, J.P. Song, Y.P. Zhang, M. Xiao, Three-field noise correlation via third-order nonlinear optical processes, Opt. Lett. 36 (2011) 2584–2586.
[13] V. Boyer, A.M. Marino, R.C. Pooser, P.D. Lett, Entangled images from four-wave mixing, Science 321 (2008) 544.
[14] Z.Z. Qin, L.M. Cao, H.L. Wang, A.M. Marino, W.P. Zhang, J.T. Jing, Experimental generation of multiple quantum correlated beams from hot rubidium vapor, Phys. Rev. Lett. 113 (2014) 023602.
[15] M.D. Lukin, A.B. Matsko, M. Fleischhauer, M.O. Scully, Quantum noise and correlations in resonantly enhanced wave mixing based on atomic coherence, Phys. Rev. Lett. 82 (1999) 1847.
[16] S.W. Du, J.M. Wen, M.H. Rubin, G.Y. Yin, Four-wave mixing and biphoton generation in a two-level system, Phys. Rev. Lett. 98 (2007) 053601.
[17] U. Khadka, Y.P. Zhang, M. Xiao, Control of multitransparency windows via dark-state phase manipulation, Phys. Rev. A 81 (2010) 023830.
[18] H.B. Zheng, Y.P. Zhang, U. Khadka, R.M. Wang, C.B. Li, Z.Q. Nie, M. Xiao, Modulating the multi-wave mixing processes via the polarizable dark states, Opt. Exp. 17 (2009) 15468.